

A GENERALIZED INFORMATION BOTTLENECK THEORY OF DEEP LEARNING

Charles Westphal¹, Stephen Hailes¹, & Mirco Musolesi^{1,2}

¹University College London, London, WC1E 6BT, UK

²University of Bologna, Bologna, Italy

{charles.westphal.21, s.hailes, m.musolesi}@ucl.ac.uk

ABSTRACT

The Information Bottleneck (IB) principle offers a compelling theoretical framework to understand how neural networks (NNs) learn. However, its practical utility has been constrained by unresolved theoretical ambiguities and significant challenges in accurate estimation. In this paper, we present a *Generalized Information Bottleneck (GIB)* framework that reformulates the original IB principle through the lens of synergy, i.e., the information obtainable only through joint processing of features. We provide theoretical and empirical evidence demonstrating that synergistic functions achieve superior generalization compared to their non-synergistic counterparts. Building on these foundations we re-formulate the IB using a computable definition of synergy based on the average interaction information (II) of each feature with those remaining. We demonstrate that the original IB objective is upper bounded by our GIB in the case of perfect estimation, ensuring compatibility with existing IB theory while addressing its limitations. Our experimental results demonstrate that GIB consistently exhibits compression phases across a wide range of architectures (including those with *ReLU* activations where the standard IB fails), while yielding interpretable dynamics in both CNNs and Transformers and aligning more closely with our understanding of adversarial robustness.

1 INTRODUCTION

Deep learning has achieved remarkable practical success, yet our theoretical understanding of how neural networks learn effective representations remains incomplete (Shwartz-Ziv & Tishby, 2017). Information theory offers a principled framework for analyzing deep learning, as information-theoretic quantities are invariant to invertible transformations and provide interpretable units of measurement (Cover & Thomas, 1991). The Information Bottleneck (IB) principle, introduced by Tishby et al. (1999), has emerged as a particularly influential framework for understanding neural network learning dynamics, providing insights into diverse phenomena including adversarial robustness (Ma et al., 2021), the effects of dropout regularization (Achille & Soatto, 2018), and generalization bounds (Kawaguchi et al., 2023). Through this interpretation, the activations of our network can be viewed as a hidden state representation \mathcal{T} , which converges to a set of statistics captured by two competing terms. The first term, referred to as the *prediction term*, quantifies the mutual information (MI) between the hidden representation \mathcal{T} and the target Y , denoted as $I(Y; \mathcal{T})$ ¹. It is straightforward to see that achieving training (and consequently test) accuracy above random guessing requires a network whose learned representation is well

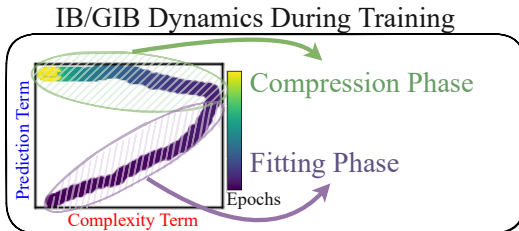


Figure 1: This schematic illustrates information plane dynamics during training, with trajectories color-coded from early epochs (light colors) to late epochs (dark purple), showing distinct fitting and compression phases.

¹For the mathematical notation used throughout this paper, see Appendix A.

aligned with that of the target data. However, it is well established that optimizing solely for prediction accuracy can lead to overfitting. Consequently, the IB framework introduces a second term: the *complexity term* $I(\mathcal{X}; \mathcal{T})$, which quantifies the mutual information between the input data \mathcal{X} and the hidden representation. Optimizing this less intuitive term can be interpreted as an effort to minimize redundant and irrelevant information from the input that is encoded in the latent space.

Overall, the IB framework posits that deep neural networks learn by solving the following Lagrangian optimization problem:

$$\mathcal{L}_{\text{IB}} = \max_{p(\mathcal{T}|\mathcal{X})} \left[\underbrace{I(\mathcal{T}; Y)}_{\text{prediction term}} - \beta^{-1} \underbrace{I(\mathcal{X}; \mathcal{T})}_{\text{complexity term}} \right] \quad (1)$$

Shwartz-Ziv & Tishby (2017) suggested that the success of deep learning can be attributed to the ability of NNs to perform the aforementioned optimization problem in two distinct phases. First, a *fitting phase*, where both of the two introduced terms increase, and second a *compression phase*, where the complexity term decreases in size (refer to Figure 1 for a visual illustration of these processes). It was argued that this second compression phase was unique to deep models and helped explain their generalizability. In some cases, the flow of information through the latent space has been shown to align precisely with the IB’s theoretical predictions (Shwartz-Ziv & Tishby, 2017).

While the IB framework initially seemed to provide a complete explanation of how neural networks balance compression and predictive accuracy, Saxe et al. (2019) presented counterexamples that challenge this view. In particular, the authors showed that compression phases depend critically on the choice of activation function: networks with *tanh* activations exhibited compression across all layers, whereas *ReLU*-based networks did not. Despite the absence of a compression phase, the *ReLU* networks still generalized well. According to Goldfeld et al. (2019), this occurs because the complexity term in deterministic networks is theoretically constant or infinite, rendering compression impossible. Consequently, the compression observed in *tanh* networks was not a genuine information-theoretic effect, but rather the result of injected randomness (Saxe et al., 2019; Shwartz-Ziv & Tishby, 2017; Geiger, 2022).

In this paper, we address these issues by introducing a generalized formulation of the IB framework that is grounded in synergy. Synergy, a concept from multivariate information theory, captures the extra predictive power that arises when inputs are considered together rather than in isolation (Williams & Beer, 2010). To motivate this perspective, we begin by asking: why synergy? We then present both theoretical arguments and empirical results showing that synergistic functions lead to improved generalization.

Having established that synergistic functions generalize better, we construct the GIB by reformulating the IB through the lens of synergy. First, we introduce a point-wise mutual information (PMI)-based reweighting scheme that ensures we measure synergy specifically for correct predictions rather than arbitrary outputs. We then combine this reweighting with our feature-wise synergy decomposition, which uses the interaction information (II) to quantify information available only through joint processing of all features. Finally, we cast this as a Lagrangian optimization problem, yielding our GIB objective that measures how synergistically the input features combine to describe correct outputs.

After deriving the GIB, we prove that, under perfect estimation, it can be lower bounded by the IB. Importantly, our formulation overcomes key theoretical limitations of standard IB, including the issue of infinite complexity terms. We demonstrate that GIB exhibits clear compression phases and interpretable learning dynamics across a wide range of scenarios where standard IB fails. In Figure 2, we revisit the experiments presented in Saxe et al. (2019) and show that the GIB displays compression phases for five different activation functions while the IB is limited to one². Beyond

²**Reading Information Planes Plots.** Throughout, we visualize information dynamics using information plane plots. In these plots, the x -axis represents the complexity term and the y -axis represents the prediction term. For standard IB, these are $I(\mathcal{X}; \mathcal{T})$ and $I(\mathcal{T}; Y)$, respectively. For the full formulation of the GIB, see Section 3. Trajectories are color-coded by training epoch, progressing from early training (dark pink/blue) to late training (light green/yellow). Blue trajectories correspond to the standard IB dynamics, whereas pink trajectories depict the dynamics under our GIB formulation. Movement leftward indicates compression (reduction of redundant information), while movement upward indicates improved prediction. For the IB we only report the information plane of the final layer as this is where compression dynamics are most readily observed. Meanwhile, the GIB

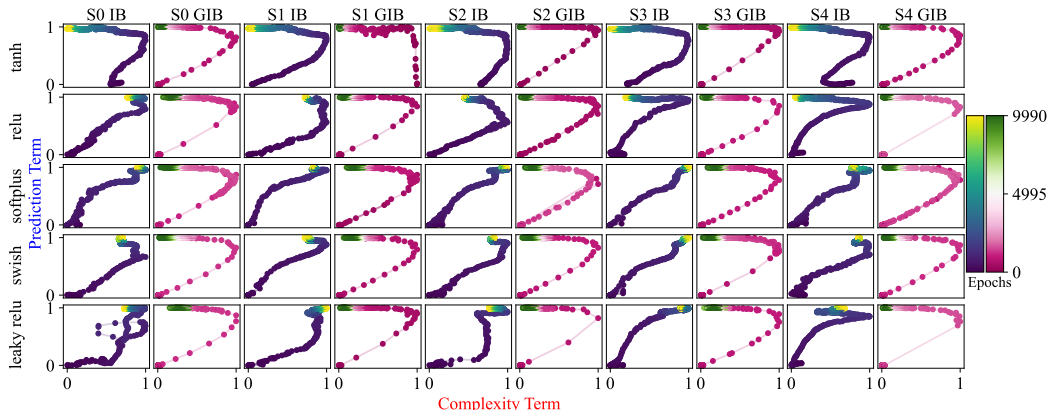


Figure 2: Information plane dynamics across multiple activation functions, extending Shwartz-Ziv & Tishby (2017) and Saxe et al. (2019) beyond *tanh* and *ReLU* to include *softplus*, *swish*, and *leaky ReLU*. Standard IB (blue) shows compression only for *tanh*; GIB (pink) shows compression for all activation functions. Each column represents one seed.

these synthetic examples, we observe consistent information dynamics in practical deep learning settings including ResNets on CIFAR-10 and BERT fine-tuning. Furthermore, the complexity term in our framework provides meaningful insights into model behavior under adversarial attacks, correctly tracking vulnerability where standard IB fails. Code for full reproducibility of these results will be made publicly available upon publication.

2 RELATED WORK

MI Estimation. MI estimation in the IB framework remains an active area of research and debate. Numerous estimators exist (e.g., k -nearest-neighbor (kNN) methods (Kozachenko & Leonenko, 1987; Kraskov et al., 2004), and kernel-density approaches (Kandasamy et al., 2015; Han et al., 2017)), and trainable neural estimators (Belghazi et al., 2018)), yet many information-theoretic studies of deep networks (Shwartz-Ziv & Tishby, 2017; Saxe et al., 2019) discretize neuron outputs (“binning”) to approximate MI. Binning is simple and fast, but even moderate coarse-graining can introduce substantial estimation error (Goldfeld et al., 2019). Despite these limitations, we use binning because MI estimates are needed throughout training (e.g., at each epoch); running kNN, KDE, or variational estimators at this frequency would be prohibitively slow and numerically unstable in high-dimensional settings. Our goal is to track relative trends in MI rather than obtain exact differential values, and binning provides a tractable, reproducible proxy that makes per-training-step MI monitoring feasible.

Other Generalizations of the Information Bottleneck. There exist many extensions of the IB framework that move beyond the original two-variable setting. For instance, the Variational IB introduces stochastic neural parameterizations to scale IB to deep networks (Alemi et al., 2017), while Information Dropout applies a neuron-wise IB-like penalty to improve generalization (Achille & Soatto, 2018). More recent work has drawn connections between IB and the framework of Partial Information Decomposition (PID), with Kolchinsky et al. (2019); Kolchinsky (2024) showing that redundancy can be isolated via an IB-style optimization. However, the work most closely related to ours is the multivariate IB of Friedman et al. (2001), which explicitly captures structure within the latent space by introducing multiple bottleneck variables and using graphical models to specify both compression and preservation relations among them. This enables the IB to consider how inputs interact to describe latent representations. While Friedman et al. (2001) multivariate IB captures statistical dependencies between multiple bottleneck variables, it does not explicitly quantify or optimize for synergistic information processing. Our approach fundamentally differs by directly measuring the information available only through collective feature processing, which we posit is key to understanding generalization in deep networks.

is formulated based on inputs and therefore only produces one information plane per training. For clarity of presentation, we normalize the complexity term and prediction term results between 0 and 1.

Synergy. Synergy characterizes the additional information obtained by evaluating variables collectively rather than individually, quantifying how features interact to reduce uncertainty about a target. The characteristics of this relationship can be illustrated by means of the XOR function. Consider two binary string variables, X_1 and X_2 , with Z being their XOR output. In this scenario, X_1 and Z , as well as X_2 and Z , are uncorrelated ($I(X_1; Z) = I(X_2; Z) = 0$), but together, X_1 and X_2 fully describe Z ($I(X_1, X_2; Z) = H(Z)$) (Guyon & Elisseeff, 2003; Williams & Beer, 2010). While the concept is intuitive, its formalization has proven challenging, leading to multiple proposed measures. Early work by Williams & Beer (2010) introduced PID, which decomposes MI into unique, redundant, and synergistic components. However, the number of terms in this decomposition equals the $n - 1$ 'th Dedekind number, where n is the number of features. This number is impractically large: a system with nine variables would require approximately 5×10^{22} terms, while for ten variables, the Dedekind number remains unknown. Moreover, estimating these terms is subject to convergence issues and size limitations (Makkeh et al., 2018; 2019; Pakman et al., 2021). While Varley & Hoel (2022) reduced the number of investigable quantities by averaging contributions of layers in the PID lattice, with different layers representing different levels of redundancy or synergy, calculations remained too complex for applications involving more than a few features. Alternative measures such as O-information (Rosas et al., 20019), correlational importance (Nirenberg & Latham, 2003), and synergistic MI (Griffith & Koch, 2014) can estimate the synergy or redundancy of large sets of variables, but fail to reveal whether a specific feature interacts synergistically or redundantly. We resolve these issues by averaging the interaction information of each feature with those remaining:

$$\text{Syn}(\mathcal{X} \rightarrow Y) = I(\mathcal{X}; Y) - \frac{1}{N} \sum_{i=1}^N (I(\mathcal{X}^{-i}; Y) + I(X^i; Y)) \quad (2)$$

where $\mathcal{X}^{-i} = \mathcal{X} \setminus \{X^i\}$. This formulation captures how features collectively reduce uncertainty about the target Y , while maintaining computational feasibility by avoiding the exponential explosion of subset calculations (Westphal et al., 2025).

3 THE GENERALIZED INFORMATION BOTTLENECK

We now introduce the GIB, by first showing that, given two functions with identical mutual information (MI) with noisy training data, the function exhibiting higher synergy achieves tighter generalization bounds. This result motivates the principle that synergistic functions generalize better than non-synergistic ones, and thus learning should favor synergy. At the same time, we emphasize that functions must also be correct. To capture this, we introduce a distribution that prioritizes accurate predictions. The final formulation of the GIB therefore maximizes the synergistic contribution of the inputs in describing this distribution.

3.1 SYNERGY AND GENERALIZATION

In this subsection, we formally establish the connection between synergy and generalization. We begin by presenting theoretical results supported by experiments on synthetic data, and then extend the discussion to empirical findings on ResNets.

3.1.1 THEORETICAL EVIDENCE

Let us first suppose we have some noise ε that can be considered independent of our input data \mathcal{X} . Now consider two functions s^- and s^+ . If s^+ combines the independent components of its arguments in a more synergistic manner than s^- , by definition we have:

$$\begin{aligned} I(s^+(\mathcal{X}, \varepsilon); \mathcal{X}, \varepsilon) - I(s^+(\mathcal{X}, \varepsilon); \varepsilon) - I(s^+(\mathcal{X}, \varepsilon); \mathcal{X}) > \\ I(s^-(\mathcal{X}, \varepsilon); \mathcal{X}, \varepsilon) - I(s^-(\mathcal{X}, \varepsilon); \varepsilon) - I(s^-(\mathcal{X}, \varepsilon); \mathcal{X}). \end{aligned} \quad (3)$$

If we now assume that $I(s^+(\mathcal{X}, \varepsilon); \mathcal{X}, \varepsilon) = I(s^-(\mathcal{X}, \varepsilon); \mathcal{X}, \varepsilon)$ (which can crudely be thought of as approximately equal train accuracies) then it must be true that:

$$I(s^+(\mathcal{X}, \varepsilon); \varepsilon) + I(s^+(\mathcal{X}, \varepsilon); \mathcal{X}) < I(s^-(\mathcal{X}, \varepsilon); \varepsilon) + I(s^-(\mathcal{X}, \varepsilon); \mathcal{X}) \quad (4)$$

where $I(s(\mathcal{X}, \varepsilon); \varepsilon)$ represents the MI between the output of a function and the noise, while $I(s(\mathcal{X}, \varepsilon); \mathcal{X})$ describes the information shared between the output and uncorrupted input. In Figure

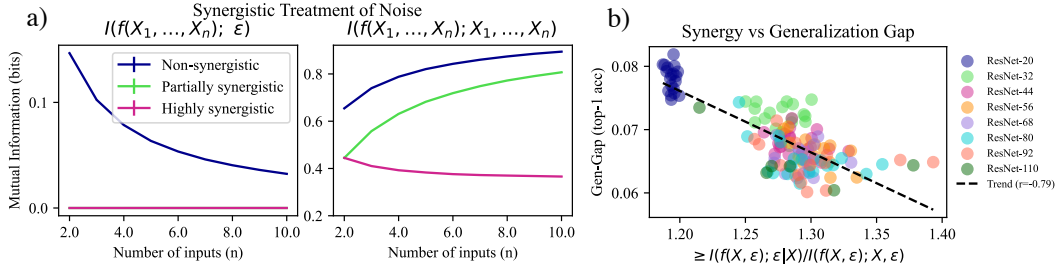


Figure 3: Synergistic processing of noise enhances generalization. (a) Controlled synthetic experiment demonstrating how synergy affects information flow (see Appendix E.1 for details). Three functions of increasing synergy process binary inputs with noise: non-synergistic (blue), partially synergistic (green), and highly synergistic (magenta). Left: $I(f(X, \varepsilon); \varepsilon)$: more synergistic functions have lower dependence on noise. Right: $I(f(X, \varepsilon); X)$ - we observe that synergistic functions have lower MI with the input. (b) Empirical validation on CIFAR-10 using ResNets of varying depths (see Appendix E.2). We quantify synergistic interactions between inputs and noise as $I(f(X, \varepsilon); \varepsilon|X)/I(f(X, \varepsilon); X, \varepsilon)$. Higher synergy correlates with smaller generalization gaps.

3(a) we analyze the implications of Equation 4 via synthetic data. We show that more synergistic functions for the same complexity of input and output have lower values of both $I(s(\mathcal{X}, \varepsilon); \varepsilon)$ and $I(s(\mathcal{X}, \varepsilon); \mathcal{X})$. This is favorable as both of these terms are known to be inversely related to generalization capabilities, as discussed below.

How $I(s(\mathcal{X}, \varepsilon); \mathcal{X})$ Impedes Generalizability. This quantity can be re-written as the complexity term of the IB, reducing its value has repeatedly been shown to be related to compression and generalization (Tishby et al., 1999; Shwartz-Ziv & Tishby, 2017). High values of this term ensure a latent representation that has memorized irrelevant and redundant information in the input. Furthermore, recent work has formally related this quantity to generalization bounds (Kawaguchi et al., 2023).

How $I(s(\mathcal{X}, \varepsilon); \varepsilon)$ Impedes Generalizability. The relationship between noise sensitivity and generalization is fundamentally tied to function smoothness. Most generalization bounds require that the learned function be *Lipschitz smooth*, meaning there exists a constant L such that $\|f(x_1) - f(x_2)\| \leq L\|x_1 - x_2\|$ for all inputs. This constraint ensures the function’s output changes at most proportionally to input perturbations. When a function has high mutual information with noise $I(s(\mathcal{X}, \varepsilon); \varepsilon)$, it indicates the output varies significantly with small noise perturbations, implying a large Lipschitz constant. As shown by Bartlett et al. (2017) and Neyshabur et al. (2017), generalization bounds scale with the Lipschitz constant of neural networks, which can be bounded by the product of layer-wise spectral norms. Therefore, functions with lower $I(s(\mathcal{X}, \varepsilon); \varepsilon)$ exhibit smaller Lipschitz constants and tighter generalization bounds, explaining why synergistic functions that minimize noise sensitivity achieve superior generalization.

3.1.2 EMPIRICAL EVIDENCE

To empirically validate our theoretical findings, we conducted experiments examining how synergistic processing of noise affects generalization in deep NNs. We trained ResNet models of varying depths (20, 32, 44, 56, 68, 80, 92, and 110 layers) on CIFAR-10 with standard data augmentations. To quantify synergy with augmentation noise, we developed a novel teacher-student framework: a teacher model trained with augmentations (random crops and horizontal flips) teaches a student model to predict its outputs from non-augmented inputs. The cross-entropy loss achieved by the student provides a maximal upper bound for the proportion of information between inputs and outputs that cannot be explained without considering the interaction of noise and features, formally: $I(f(X, \varepsilon); \varepsilon|X)/I(f(X, \varepsilon); X, \varepsilon)$.

Our results, shown in Figure 3(b), reveal a strong negative correlation (Pearson $r = -0.79$, $p < 0.001$) between this synergy measure and generalization performance across all model configurations. Models with higher synergy (those whose predictions depend more on the interaction between image content and augmentation patterns) consistently achieve smaller generalization gaps. This confirms our theoretical prediction: synergistic processing of augmentation noise, rather than treating it as independent corruption, enables models to extract more robust features that generalize better

to clean test images. Full experimental details are provided in Appendix E.2. Considering that to synergistically process noise, we must synergistically process the features, we design our GIB principle based on measures of feature synergy.

3.2 FORMULATING THE GIB PRINCIPLE

During the last section, we argued that synergistic functions generalize better than their non-synergistic counterparts. Consequently, we argue that when learning, a deep network should aim to maximize the synergy of the inputs to produce the outputs. However, this is not a strict enough condition, because there are many different synergistic functions, most of which are irrelevant to the task at hand. We instead want to measure how synergistically our inputs combine to give the *correct* outputs.

To facilitate this, we define a new distribution that, instead of describing Z our output, describes the co-occurrences of Z with Y . The exact definition of $Q(Z, Y)$ is based on PMI-based reweighting, i.e., weighting samples by the likelihood ratio between the joint distribution and the product of marginals: $Q(Z, Y) = \frac{P(Z, Y)}{P(Z)P(Y)}$. This reweighting scheme emphasizes patterns where Z and Y co-occur more frequently than would be expected under independence, effectively highlighting the meaningful dependencies between our learned representations and the target outputs. PMI has proven effective in capturing meaningful associations in numerous ML contexts: it underlies word2vec’s implicit matrix factorization (Levy & Goldberg, 2014), drives contrastive learning objectives (van den Oord et al., 2018), and measures feature relevance in interpretable ML (Bouma, 2009). Combining this definition with how we earlier defined synergy, we get the following formulation of the GIB:

$$\mathcal{L}_{\text{GIB}} = \max_{p(Z|X)} [\text{Syn}(\mathcal{X} \rightarrow Q(Z, Y))] \quad (5)$$

$$= \max_{p(Z|X)} \left[\underbrace{I(\mathcal{X}; Q(Z, Y))}_{\text{prediction term}} - \underbrace{\frac{1}{2\beta N} \sum_{i=1}^N (I(\mathcal{X}^{-i}; Q(Z, Y)) + I(\mathcal{X}^i; Q(Z, Y)))}_{\text{complexity term}} \right] \quad (6)$$

The prediction term (blue) $I(\mathcal{X}; Q(Z, Y))$ measures the mutual information between all input features and the PMI-reweighted distribution, capturing how well the complete feature set predicts patterns where model outputs and true labels co-occur beyond chance. The complexity term (red) $\frac{1}{2\beta N} \sum_{i=1}^N (I(\mathcal{X}^{-i}; Q(Z, Y)) + I(\mathcal{X}^i; Q(Z, Y)))$ inversely quantifies the average information obtainable from individual features or their complements. By maximizing their difference, GIB measures information dynamics that emerge only from collective feature interactions, which our analysis also indicates leads to improved generalization. On the other hand, measuring synergy can be computationally demanding, as we discuss in Appendix G.

4 RELATING THE GIB TO THE IB

In this section, we first prove that under a simple assumption (i.e., perfect estimation) the IB is a lower bound of our GIB. Finally, we discuss how the GIB solves longstanding IB issues.

Theorem 1. *If we assume perfect training accuracy and therefore $Q(Z, Y) = Z = Y$, then the original IB objective is upper bounded by our GIB:*

$$I(\mathcal{T}; Y) - \beta I(\mathcal{X}; \mathcal{T}) \leq I(\mathcal{X}; Q(Z, Y)) - \frac{1}{2\beta N} \sum_{i=1}^N (I(\mathcal{X}^{-i}; Q(Z, Y)) + I(\mathcal{X}^i; Q(Z, Y))) \quad (7)$$

The proof is provided in Appendix B. This result demonstrates that the GIB provides an upper bound on the IB objective. Consequently, as we optimize the traditional IB to find sufficient statistics, we simultaneously optimize our GIB objective, ensuring that our approach remains compatible with the theoretical foundations of the IB. For instance, in Appendix C we prove the GIB discovers sufficient statistics.

This new formulation overcomes two main limitations of the original IB. First, the partition across subsets of features combined with the PMI definition of $Q(Z, Y)$ protects the compression term

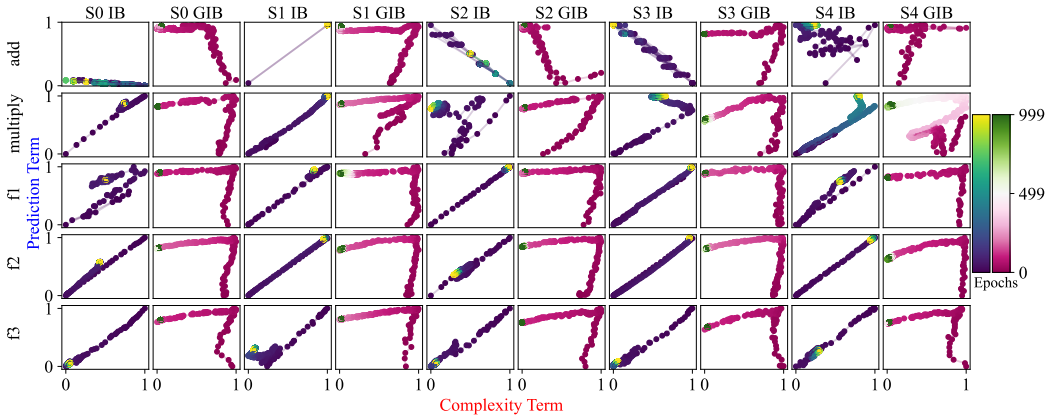


Figure 4: Information plane dynamics for NNs learning simple mathematical functions. Comparison of standard IB versus GIB across five functions (rows) and five random seeds. Functions include basic arithmetic and symmetric polynomials. GIB consistently shows compression phases (leftward movement), while standard IB exhibits varied behaviors. See Appendix E.3 for experimental details.

from becoming infinite. In Appendix D we prove that the GIB is only infinite under interpretable circumstances. Second, and more fundamentally, our formulation explicitly considers over-reliance on individual features, as explained in Section 3.1. IB optimizes the total information flow between inputs and outputs through the latent representation \mathcal{T} without considering how features interact. In contrast, GIB explicitly models how inputs combine to form the latent representation, distinguishing between different types of feature interactions. This is evident in the complexity terms: IB’s $\beta^{-1}I(\mathcal{X}; \mathcal{T})$ aggregates all information equally, while GIB’s synergistic decomposition $\frac{1}{2\beta N} \sum_{i=1}^N (I(\mathcal{X}^{-i}; Q(Z, Y)) + I(X^i; Q(Z, Y)))$ penalizes the information contained in individual features. Consequently, IB compresses indiscriminately, whereas GIB selectively preserves long-range feature combinations; the synergistic patterns we have shown lead to better generalization.

5 EXPERIMENTAL CASE STUDIES

This section presents experimental evidence demonstrating GIB’s advantages over standard IB across diverse settings. We show that GIB provides more consistent and interpretable information dynamics throughout training, successfully capturing compression phases where standard IB fails (refer to Footnote 2 on reading information planes). Additionally, we demonstrate that GIB’s complexity term serves as a direct indicator of adversarial vulnerability, providing quantitative insights into model robustness that standard IB cannot capture. As stated in Section 2, all MIs will be estimated using binning. However, in Appendix F, we reproduce our results with a different method of MI estimation.

5.1 INFORMATION DYNAMICS OF MLPs LEARNING SIMPLE FUNCTIONS

We examine NNs learning five mathematical functions of increasing complexity: addition, multiplication, and three symmetric polynomials labelled f1, f2 and f3 (polynomials in which all arguments are subjected to the same operations). Full experimental details are in Appendix E.3.

The information plane dynamics in Figure 4 show clear differences between the standard IB and GIB formulations. For the GIB, we observe compression phases, characterized by leftward movement during training, across all five functions and random seeds. The trajectories initially move upward and rightward as networks fit the training data, then shift leftward as training progresses. The standard IB displays more variable behavior, without real indication of compression, despite the strong generalization capabilities of these networks.

5.2 INFORMATION DYNAMICS OF RESNETS

We analyze information dynamics in residual networks (ResNets) of varying depths (20, 56, 80, 110 layers) trained on CIFAR-10. For the standard IB, we compute MI using the 10-dimensional

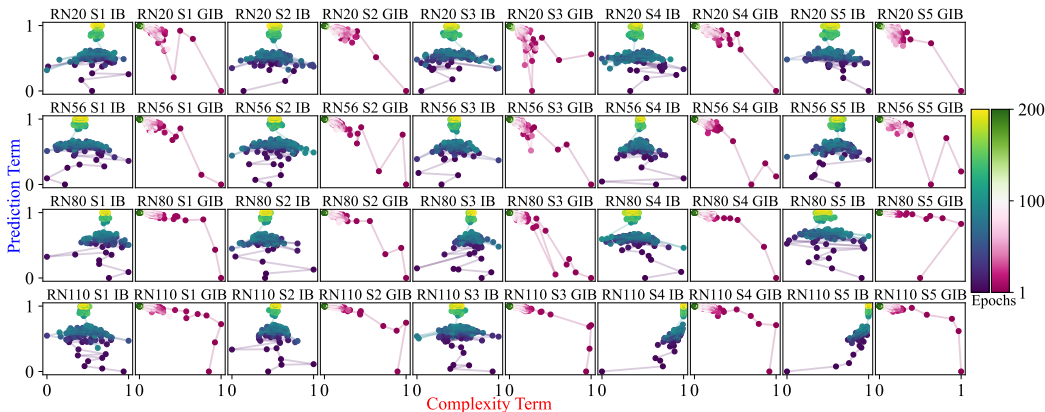


Figure 5: Information plane dynamics for ResNets of varying depths trained on CIFAR-10. Comparison across four network depths and five random seeds. GIB consistently exhibits compression phases, while standard IB shows limited or no compression. See Appendix E.4 for details.

output layer directly. For GIB, due to the need to compute feature-wise decompositions on the high-dimensional input space (3072 dimensions), we first apply Kernel PCA to reduce the pixel space to 50 principal components before computing MI, as explained in more detail in Appendix E.4 (Turk & Pentland, 1991). For more details as to why we chose 50 components, see Appendix H.

Figure 5 displays information plane trajectories for ResNets trained on CIFAR-10. The GIB formulation shows consistent compression behavior across all network depths and random seeds, though the dynamics vary with architecture size. In smaller networks (ResNet-20), trajectories show a general trend of increasing prediction term while the complexity term decreases throughout training. Larger networks (ResNet-56 and above) begin to show more pronounced phase structure.

The standard IB presents markedly different dynamics. Rather than showing clear phases, IB trajectories remain largely clustered with minimal directional movement across epochs. The absence of compression phases in standard IB holds across all tested architectures, confirming previous observations that *ReLU* networks fail to exhibit expected IB behavior (Saxe et al., 2018).

5.3 INFORMATION DYNAMICS OF TRANSFORMERS CLASSIFYING NEWS HEADLINES

We examine BERT-base fine-tuned on AG News text classification, comparing standard fine-tuning with a novel “unlearning” initialization strategy. In this case, unlearning involves training on random labels to remove biases from the model. For the standard IB, we again set \mathcal{T} as the final layer representation for use in MI calculations. For GIB, we apply our feature-wise synergy decomposition to the full set of inputs. Full experimental details are in Appendix E.5.

The standard fine-tuning approach shown in row 1 of Figure 6 produces highly variable trajectories that begin near the center of the information plane, indicating that pre-trained BERT representations contain substantial pre-training biases. This prompted us to unlearn, where we train on random labels. The unlearning intervention dramatically alters these dynamics. After 3 epochs of random label training, models consistently start from the bottom-right corner of the information plane, as shown in row 2. From this reset position, both IB and GIB show more coherent learning trajectories during subsequent fine-tuning. This reveals how studying these information-planes can be used for diagnostics and interpretation. It is worth noting that, in the absence of unlearning for seed 2, the model failed to overcome its initial biases, which led to atypical and unstable information dynamics.

5.4 ADVERSARIAL ROBUSTNESS

We investigate how adversarial perturbations affect information dynamics by training NNs with *tanh* activations on MNIST under Fast Gradient Sign Method (FGSM) attacks of varying strength. Full details are in Appendix E.6. Figure 7(a) illustrates the effect of adversarial attacks on learning dynamics. Networks trained under weak attacks ($\epsilon = 0.01$) exhibit normal convergence, whereas strong attacks ($\epsilon = 1.0$) substantially hinder the learning process. The information-theoretic analysis

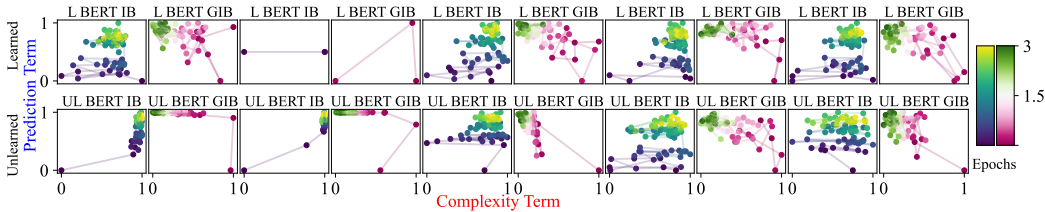


Figure 6: Information plane dynamics for BERT fine-tuned on AG News. Comparison of standard fine-tuning (top) versus unlearning + fine-tuning (bottom). The unlearning procedure repositions models to a more favorable initialization point for subsequent learning. See Appendix E.5 for details.

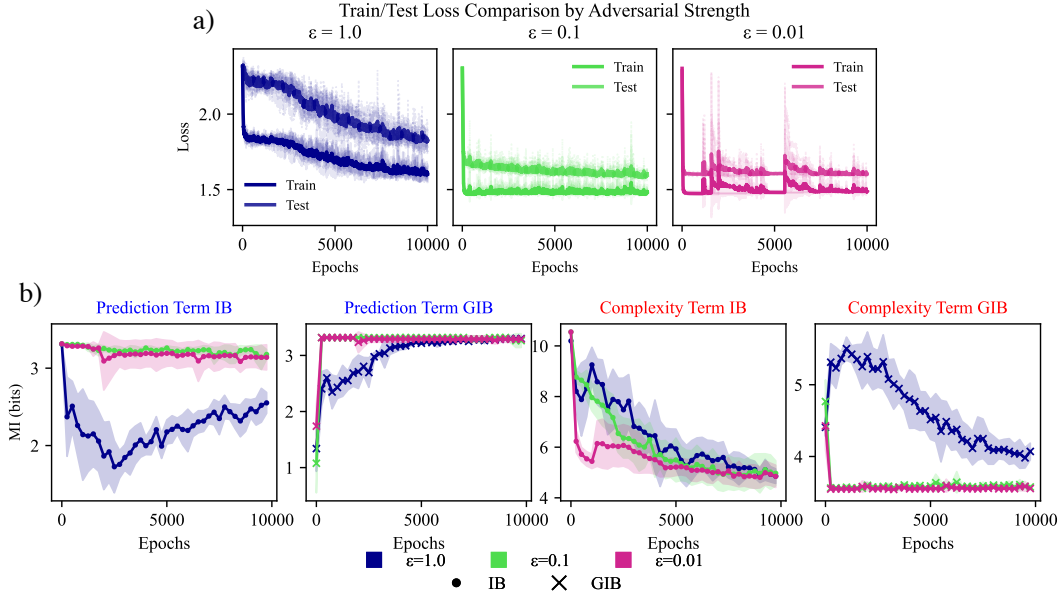


Figure 7: Information dynamics under adversarial attacks on MNIST. (a) Training dynamics for three FGSM attack strengths. (b) Information-theoretic analysis comparing IB versus GIB. GIB’s complexity term correctly reflects degradation in generalization, while standard IB fails to differentiate between attack strengths. See Appendix E.6 for details.

in Figure 7(b) exposes a critical difference between standard IB and our GIB formulation. The GIB’s complexity term faithfully reflects the degradation in generalization: values remain high for $\epsilon = 1.0$ (poor generalization), while decreasing rapidly when proper training occurs. In contrast, the standard IB’s complexity term shows minimal differentiation between attack strengths.

6 CONCLUSION

In this work, we have introduced the Generalized Information Bottleneck (GIB), a principled reformulation of the IB that explicitly accounts for synergistic interactions between features. Our theoretical and empirical analysis demonstrated that synergistic functions achieve better generalization, providing a fundamental justification for why deep networks should learn representations that combine inputs synergistically rather than processing them independently. The GIB framework addresses several longstanding limitations of the original IB. First, we proposed a PMI-based reweighting scheme $Q(Z, Y)$ that protects the compression term from becoming infinite during training. Second, we have introduced a feature-wise synergy decomposition, explicitly penalizing representations that rely too heavily on individual features or simple feature combinations. This ensures that our formulation highlights when networks learn patterns that emerge solely through the collective processing of multiple inputs, a distinction that is crucial for robust generalization. Our experimental results across diverse architectures demonstrate that GIB provides a more complete picture of how deep networks process information. The GIB framework opens new possibilities for both understanding and improving deep learning systems.

REFERENCES

- Alessandro Achille and Stefano Soatto. Information dropout: Learning optimal representations through noisy computation. *IEEE Transactions on Pattern Analysis and Machine Intelligence*, 40(12):2897–2905, 2018.
- Alexander A. Alemi, Ian Fischer, Joshua V. Dillon, and Kevin Murphy. Deep variational information bottleneck. In *Proceedings of the 5th International Conference on Learning Representations (ICLR’17)*, 2017.
- Peter L. Bartlett, Dylan J. Foster, and Matus J. Telgarsky. Spectrally-normalized margin bounds for neural networks. In *Advances in Neural Information Processing Systems (NeurIPS’17)*, 2017.
- Mohamed Ishmael Belghazi, Aristide Baratin, Sai Rajeshwar, Sherjil Ozair, Yoshua Bengio, Aaron Courville, and R. Devon Hjelm. Mutual information neural estimation. In *Proceedings of the 35th International Conference on Machine Learning (ICML’18)*, 2018.
- Anthony J Bell. Co-information lattice. In *Proceedings of the 4th International Symposium on Independent Component Analysis and Blind Source Separation*, pp. 921–926, 2003.
- Gerlof Bouma. Normalized (pointwise) mutual information in collocation extraction. In *Proceedings of the 21st Biennial Gesellschaft für Semantische Verarbeitung Natürlicher Sprache Conference (GSCL’09)*, 2009.
- Thomas M. Cover and Joy A. Thomas. *Elements of Information Theory*. Wiley-Interscience, New York, 1st edition, 1991. ISBN 978-0471062592.
- Ian C. Covert, Scott Lundberg, and Su-In Lee. Understanding global feature contributions with additive importance measures. In *Advances in Neural Information Processing Systems (NeurIPS’20)*, 2020.
- Nir Friedman, Ori Mosenzon, Noam Slonim, and Naftali Tishby. Multivariate information bottleneck. In *Proceedings of the 17th Conference on Uncertainty in Artificial Intelligence (UAI’01)*, 2001.
- Bernhard C. Geiger. On information plane analyses of neural network classifiers – a review. *IEEE Transactions on Neural Networks and Learning Systems*, 33(12):7039–7051, 2022.
- Ziv Goldfeld, Ewout van den Berg, Kristjan Greenewald, Igor Melnyk, Nam Nguyen, Brian Kingsbury, and Yury Polyanskiy. Estimating information flow in deep neural networks. *Proceedings of the 36th International Conference on Machine Learning (ICML’19)*, 2019.
- Virgil Griffith and Christof Koch. Quantifying synergistic mutual information. In Mikhail Prokopenko (ed.), *Guided Self-Organization: Inception*, pp. 159–190. Springer, 2014.
- Isabelle Guyon and André Elisseeff. An introduction to variable and feature selection. *Journal of Machine Learning Research*, 3:1157–1182, 2003.
- Yanjun Han, Jiantao Jiao, and Tsachy Weissman. Differential entropy estimation via score matching. In *International Conference on Artificial Intelligence and Statistics (AISTAT’17)*, 2017.
- Kirthevasan Kandasamy, Akshay Krishnamurthy, and Barnabas Poczos. Nonparametric von Mises estimators for entropies, divergences and mutual informations. In *Advances in Neural Information Processing Systems (NeurIPS’15)*, 2015.
- Kenji Kawaguchi, Zhun Deng, Xu Ji, and Jiaoyang Huang. How does information bottleneck help deep learning? In *Proceedings of the 40th International Conference on Machine Learning (ICML’23)*, 2023.
- Artemy Kolchinsky. Partial information decomposition: Redundancy as information bottleneck. *Entropy*, 26(7):1–20, 2024.
- Artemy Kolchinsky, Brendan D. Tracey, and David H. Wolpert. Nonlinear information bottleneck. *Entropy*, 21(12):1181, 2019.

- L. F. Kozachenko and N. N. Leonenko. The sample estimate of the entropy of a random vector. *Problemy Peredachi Informatsii*, 23(2):9–16, 1987.
- Alexander Kraskov, Harald Stögbauer, and Peter Grassberger. Estimating mutual information. *Physical Review E*, 69(6):066138, 2004.
- Omer Levy and Yoav Goldberg. Neural word embedding as implicit matrix factorization. In *Advances in Neural Information Processing Systems (NeurIPS'14)*, pp. 2177–2185, 2014.
- Chao Ma, Chen Zhang, and Liwei Wang. Revisiting Hilbert-Schmidt information bottleneck for adversarial robustness. In *Advances in Neural Information Processing Systems (NeurIPS'21)*, 2021.
- Abdullah Makkeh, Dirk Oliver Theis, and Raul Vicente. BROJA-2PID: A robust estimator for bivariate partial information decomposition. *Entropy*, 20(4):271, 2018.
- Abdullah Makkeh, Armin J. Gutknecht, and Michael Wibral. MAXENT3D_PID: An estimator for the maximum-entropy trivariate partial information decomposition. *Entropy*, 21(9):862, 2019.
- Behnam Neyshabur, Srinadh Bhojanapalli, David McAllester, and Nati Srebro. Exploring generalization in deep learning. In *Advances in Neural Information Processing Systems (NeurIPS'17)*, 2017.
- Sheila Nirenberg and Peter E. Latham. Decoding neuronal spike trains: How important are correlations? *Proceedings of the National Academy of Sciences of the United States of America*, 100(12): 7348–7353, 2003.
- Ari Pakman, Amir Nejatbakhsh, Julien Terglane, Cengiz Pehlevan, and Liam Paninski. Estimating the unique information of continuous variables. In *Advances in Neural Information Processing Systems (NeurIPS'21)*, 2021.
- Fernando E. Rosas, Pedro A. M. Mediano, Michael Gastpar, and Henrik J. Jensen. Quantifying high-order interdependencies via multivariate extensions of the mutual information. *Physical Review E*, 100(3):032305, 20019.
- Andrew M. Saxe, Yamini Bansal, Joel Dapello, Madhu Advani, Artemy Kolchinsky, Brendan D. Tracey, and David D. Cox. On the information bottleneck theory of deep learning. *Journal of Statistical Mechanics: Theory and Experiment*, 2018.
- Andrew M. Saxe, Yamini Bansal, Joel Dapello, and Madhu Advani. On the information bottleneck theory of deep learning. *Proceedings of the 7th International Conference on Learning Representations (ICLR'19)*, 2019.
- Elad Schneidman, William Bialek, and Michael J Berry. Synergy, redundancy, and independence in population codes. *Journal of Neuroscience*, 23(37):11539–11553, 2003.
- Ravid Shwartz-Ziv and Naftali Tishby. Opening the black box of deep neural networks via information. *arXiv preprint arXiv:1703.00810*, 2017.
- Naftali Tishby, Fernando C. Pereira, and William Bialek. The information bottleneck method. In *Proceedings of the 37th Annual Allerton Conference on Communication, Control, and Computing*, 1999.
- Matthew A. Turk and Alex P. Pentland. Face recognition using eigenfaces. In *Proceedings of the 4th IEEE Computer Society Conference on Computer Vision and Pattern Recognition (CVPR'91)*, 1991.
- Aaron van den Oord, Yazhe Li, and Oriol Vinyals. Representation learning with contrastive predictive coding. *arXiv preprint arXiv:1807.03748*, 2018.
- Thomas F. Varley and Erik Hoel. Emergence as the conversion of information: A unifying theory. *Philosophical Transactions of the Royal Society A*, 380(2227):20210150, 2022.

Charles Westphal, Stephen Hailes, and Mirco Musolesi. Partial information decomposition for data interpretability and feature selection. In *Proceedings of the 28th International Conference on Artificial Intelligence and Statistics (AISTATS'25)*, 2025.

Paul L. Williams and Randall D. Beer. Nonnegative decomposition of multivariate information. In *arXiv preprint arXiv:1004.2515*, 2010.

A NOTATION TABLE

Table 1 contains all the mathematical notation used in this paper.

Table 1: Summary of Notational Conventions.

Symbol	Description
\mathcal{X}	Set of input random variables (features)
X^i	i -th individual input feature
\mathcal{X}^{-i}	All features except the i -th feature: $\mathcal{X} \setminus \{X^i\}$
Y	Target random variable (labels)
Z	Output/prediction random variable
\mathcal{T}	Hidden representation/latent space
ε	Noise random variable
N	Number of input features
β	Trade-off parameter in IB formulation
$I(\cdot; \cdot)$	Mutual information
$H(\cdot)$	Entropy
$H(\cdot \cdot)$	Conditional entropy
$P(\cdot)$	Probability distribution
$Q(Z, Y)$	PMI-based reweighted distribution
$\text{Syn}(\cdot)$	Synergy measure
s^+, s^-	More/less synergistic functions
IB	Information Bottleneck
GIB	Generalized Information Bottleneck
MI	Mutual Information
NN	Neural Network
PMI	Point-wise Mutual Information
PID	Partial Information Decomposition
FGSM	Fast Gradient Sign Method

B PROOF OF THEOREM 1

In this section we prove Theorem 1. To do this, we assume that we have perfect training performance and therefore $Q(Y, Z) = Y = Z$. We also assume the predictor is deterministic given its input (as in a standard feed-forward network), hence $H(Z|\mathcal{X}) = 0$ and therefore

$$I(\mathcal{X}; Z) = H(Z). \quad (8)$$

Proof. Given this, our GIB formulation becomes:

$$\mathcal{L}_{\text{GIB}} = I(\mathcal{X}; Q(Z, Y)) - \frac{1}{2\beta N} \sum_{i=1}^N (I(\mathcal{X}^{-i}; Q(Z, Y)) + I(\mathcal{X}^i; Q(Z, Y))) \quad (9)$$

$$= I(\mathcal{X}; Y) - \frac{1}{2\beta N} \sum_{i=1}^N (I(\mathcal{X}^{-i}; Z) + I(\mathcal{X}^i; Z)) \quad (10)$$

$$\geq I(\mathcal{X}; Y) - \frac{1}{2\beta N} \sum_{i=1}^N (H(Z) + H(Z)) \quad (\text{by monotonicity.}) \quad (11)$$

$$= I(\mathcal{X}; Y) - \frac{1}{2\beta N} \cdot N \cdot 2H(Z) \quad (12)$$

$$= I(\mathcal{X}; Y) - \frac{1}{\beta} H(Z) \quad (13)$$

$$= I(\mathcal{X}; Y) - \frac{1}{\beta} I(\mathcal{X}; Z) \quad (\text{by Eq. 8}) \quad (14)$$

$$\geq I(\mathcal{X}; Y) - \frac{1}{\beta} I(\mathcal{X}; \mathcal{T}) \quad (\text{by dpi.}) \quad (15)$$

$$\geq I(\mathcal{T}; Y) - \frac{1}{\beta} I(\mathcal{X}; \mathcal{T}) \quad (\text{by dpi.}) \quad (16)$$

$$(17)$$

We obtain:

$$I(\mathcal{T}; Y) - \frac{1}{\beta} I(\mathcal{X}; \mathcal{T}) \leq \mathcal{L}_{\text{GIB}}$$

which shows that the original IB objective is upper bounded by the proposed GIB under the stated assumption. \square

C GIB AND SUFFICIENT STATISTICS

In this section, we prove the GIB discovers sufficient statistics.

Theorem 2. *Let $(X, Y) \sim P_{X, Y}$ and let $Z \sim P_{Z|X}$ be any (possibly stochastic) encoder. Define*

$$Q(Z, Y) = \frac{P_{Z, Y}(Z, Y)}{P_Z(Z)P_Y(Y)} = \frac{P_{Z|Y}(Z|Y)}{P_Z(Z)} = \frac{P_{Y|Z}(Y|Z)}{P_Y(Y)}.$$

For $\beta \in (0, \infty]$, consider

$$\mathcal{J}_\beta(P_{Z|X}) := I(X; Q(Z, Y)) - \frac{1}{\beta 2N} \sum_{i=1}^N (I(\mathcal{X}^{-i}; Q(Z, Y)) + I(\mathcal{X}^i; Q(Z, Y))),$$

where $X = (X^1, \dots, X^N)$ and \mathcal{X}^{-i} omits coordinate i . Then, at $\beta = \infty$,

$$\sup_{P_{Z|X}} \mathcal{J}_\infty = \sup_{P_{Z|X}} I(X; Q(Z, Y)) = I(X; Y),$$

and the supremum is attained if and only if Z is sufficient for Y given X , i.e., $P_{Y|X} = P_{Y|Z}$ almost surely.

Proof. At $\beta = \infty$ the penalty vanishes and $\mathcal{J}_\infty = I(X; Q)$. The transformation $(X, Y) \mapsto (X, Q)$ is a (possibly randomized) Markov kernel induced by first drawing $Z \sim P_{Z|X}(\cdot|X)$ and then setting $Q = \frac{P_{Y|Z}(Y|Z)}{P_Y(Y)}$. By data processing for KL divergence,

$$I(X; Q(Z, Y)) \leq I(X; Y).$$

Taking the supremum over $P_{Z|X}$ yields $\sup_{P_{Z|X}} I(X; Q) \leq I(X; Y)$. From this point onward, we adopt the same analytical approach as the IB framework to demonstrate that the GIB identifies sufficient statistics. See Tishby et al. (1999). \square

D WHEN GIB ENCOUNTERS INFINITY

In this section, we analyze the conditions under which our GIB formulation yields infinite values and show that, unlike standard IB, these infinities have meaningful interpretations.

Theorem 3. *Let \mathcal{X} and Y be continuous random variables with continuous probability distributions. Assume perfect training accuracy such that $Q(Z, Y) = Z = Y$ and $H(Z|\mathcal{X}) = 0$ (deterministic predictor). If no single feature or feature subset can perfectly predict the output, i.e.,*

$$\frac{1}{N} \sum_{i=1}^N (I(\mathcal{X}^{-i}; Z) + I(X^i; Z)) < \infty,$$

then $\mathcal{L}_{\text{GIB}} = \infty$.

Proof. Starting from our GIB formulation with $Q(Z, Y) = Z = Y$:

$$\mathcal{L}_{\text{GIB}} = I(\mathcal{X}; Q(Z, Y)) - \frac{1}{2\beta N} \sum_{i=1}^N (I(\mathcal{X}^{-i}; Q(Z, Y)) + I(X^i; Q(Z, Y))) \quad (18)$$

$$= I(\mathcal{X}; Z) - \frac{1}{2\beta N} \sum_{i=1}^N (I(\mathcal{X}^{-i}; Z) + I(X^i; Z)) \quad (19)$$

$$= \infty - \frac{1}{2\beta N} \sum_{i=1}^N (I(\mathcal{X}^{-i}; Z) + I(X^i; Z)) \quad (20)$$

$$= \infty \quad (21)$$

The third line follows because $I(\mathcal{X}; Z) = \infty$ for continuous variables with perfect dependence, while the sum remains finite by assumption. \square

Interpretation of Infinities in GIB. In contrast to the original IB, where infinities arise as technical artifacts, the infinities in our GIB possess more interpretability. When $\mathcal{L}_{\text{GIB}} = \infty$, we have a case of perfect synergy: the output cannot be predicted without the complete feature set, and removing even a single feature results in loss of predictive power. This represents the ideal synergistic function where all features must interact to determine the output.

Conversely, if any single feature subset can perfectly predict the output (in violation of our assumption), then at least one of the terms $I(\mathcal{X}^{-i}; Z)$ or $I(X^i; Z)$ becomes infinite, making the entire sum infinite. In this case, $\mathcal{L}_{\text{GIB}} = \infty - \infty = 0$. Therefore, while both IB and GIB yield infinities in the continuous setting, our formulation admits a meaningful interpretation: an infinite GIB corresponds to perfect synergy, indicating that all features are essential. This contrasts with standard IB, where infinities are just a technical feature of continuous random variables under deterministic functions.

E EXPERIMENTAL SETTINGS

E.1 SYNTHETIC SYNERGY EXPERIMENT

Data Generation. For each input dimension $n \in \{2, \dots, 10\}$, we generate $N = 10^6$ samples. Each sample consists of a binary input vector $X \in \{0, 1\}^n$ with i.i.d. Bernoulli(0.5) entries. We apply a “force-to-1” noise model: with probability $p_{\text{flip}} = 1/3$, we randomly select one coordinate $i \sim \text{Uniform}\{1, \dots, n\}$ and set $X'_i = 1$, leaving all other coordinates unchanged. With probability $2/3$, no modification is made ($X' = X$). The noise pattern is encoded as $\varepsilon \in \{0, 1, \dots, n\}$, where 0 indicates no flip and $i > 0$ indicates coordinate i was forced to 1.

Functions. We examine three deterministic functions of increasing synergy applied to the noisy input X' :

- Non-synergistic: $f_1(X') = X'_1$ (output depends only on first input)
- Partially synergistic: $f_2(X') = X'_1 \oplus X'_2$ (XOR of first two inputs)
- Highly synergistic: $f_3(X') = \bigoplus_{i=1}^n X'_i$ (XOR of all inputs)

MI Estimation. Since all variables are discrete, we compute exact MI using empirical probability distributions with base-2 logarithms.

E.2 CIFAR-10 SYNERGY WITH AUGMENTATION

Architecture and Training. We train ResNet models of depths {20, 32, 44, 56, 68, 80, 92, 110} on CIFAR-10. Each architecture follows the standard ResNet design for CIFAR with initial 3×3 convolution, three residual stages, global average pooling, and a final 10-way linear classifier. Models are trained with SGD (learning rate 0.1, momentum 0.9, weight decay 5×10^{-4}) for 200 epochs with batch size 256. Learning rate is reduced by a factor of 0.1 at epochs 100 and 150 using MultiStepLR scheduler. Standard data augmentation consists of random crops (32×32 with padding 4) and horizontal flips applied during training.

Teacher-Student Framework. To quantify synergy with augmentation noise, we employ a two-stage approach. First, a teacher network is trained as described above on augmented data. After training, we collect the teacher’s softmax outputs on the augmented training set. We then train a student network of identical architecture to predict these teacher outputs from non-augmented inputs. The student is trained for 200 epochs using the same SGD configuration (lr=0.1, momentum=0.9, weight decay= 5×10^{-4}) with MultiStepLR milestones at epochs 100 and 150. The student minimizes cross-entropy loss between its predictions and the teacher’s softmax targets.

Synergy Measurement. We compute the marginal entropy of teacher predictions as $H(Y) = -\mathbb{E}[(p_{\text{teacher}} \log p_{\text{teacher}})]$ where the expectation is over all augmented training samples. The conditional entropy is estimated as the final cross-entropy loss achieved by the converged student model. The synergy ratio $I(f(X, \varepsilon); \varepsilon|X)/I(f(X, \varepsilon); X, \varepsilon)$ (which can be re-written as the final loss of the student divided by the total entropy) quantifies the proportion of the teacher’s output entropy that cannot be predicted from clean images alone, requiring knowledge of the augmentation pattern.

E.3 SIMPLE FUNCTIONS

Network Architecture. All networks consist of a single hidden layer with specified units, followed by a linear output layer. No bias terms, regularization, or normalization are used. Weights are initialized using PyTorch’s default settings, namely Kaiming uniform for the hidden layers and uniform initialization for the output layer.

Target Functions and Architectures. The target functions and architectures considered in our evaluation are the following:

- Addition: $f(a, b) = a + b$, 2 inputs \rightarrow 4 hidden units (identity activation) \rightarrow 1 output;
- Multiplication: $f(a, b) = a \times b$, 2 inputs \rightarrow 3 hidden units (square activation: x^2) \rightarrow 1 output;
- Symmetric polynomial 1 (f1): $f(a, b, c) = ab + bc + ca$, 3 inputs \rightarrow 16 hidden units (square activation: x^2) \rightarrow 1 output;
- Symmetric polynomial 2 (f2): $f(a, b, c) = a^2 + b^2 + c^2$, 3 inputs \rightarrow 8 hidden units (square activation: x^2) \rightarrow 1 output;
- Symmetric polynomial 3 (f3): $f(a, b, c, d) = ab + bc + cd + da$, 4 inputs \rightarrow 16 hidden units (square activation: x^2) \rightarrow 1 output.

Training Details. Networks are trained with standard gradient descent (no momentum) with learning rate 0.01 for 1000 epochs, minimizing mean squared error (MSE) loss. Training data consists of 1500 samples uniformly sampled from $[-10, 10]^n$ for all functions except addition, which uses $[0, 10]^2$. Test data uses 1500 samples from the extended range $[-1000, 1000]^n$ to evaluate extrapolation. MI is computed every 10 epochs using histogram binning with 40 bins. We get our binning estimation technique from Saxe et al. (2018).

E.4 RESNETS ON CIFAR-10

Architecture. We use standard ResNet architectures for CIFAR-10 with depths $\{20, 56, 80, 110\}$, implemented with BasicBlocks. Each network has an initial 16-filter 3×3 convolution, followed by three stages with $\{16, 32, 64\}$ filters respectively, global average pooling, and a 10-way linear classifier.

Training. Models are trained on CIFAR-10 (50k train, 10k test) with SGD (momentum 0.9, weight decay 5×10^{-4} , initial learning rate 0.1) for 200 epochs with batch size 128. Learning rate decays by 0.1 at epochs 100 and 150. Standard augmentation includes random crops (32×32 , padding 4) and horizontal flips. No additional preprocessing is applied beyond standard CIFAR normalization.

MI Estimation. For standard IB, we compute MI between the 10-dimensional logit vector \mathcal{T} (pre-softmax outputs) and targets Y . For GIB’s input decomposition, we first apply Kernel PCA with RBF kernel ($\gamma=1/3072$) to reduce the 3072-dimensional flattened images to 50 principal components. MI is computed at each epoch using the first 5000 training samples with histogram binning (30 bins). For IB: $I(\mathcal{T}; Y)$ using the 10-dimensional logits. For GIB: synergy decomposition using the 50 PCA components as features.

E.5 BERT ON AG NEWS

Model Configuration. BERT-base-uncased (12 layers, 768 hidden dimensions, 12 attention heads) fine-tuned for 4-way AG News classification (World, Sports, Business, Sci/Tech). The dataset contains 120,000 training and 7,600 test examples. Maximum sequence length is 128 tokens with padding.

Training Protocols. The training protocols used in our evaluation are the following:

- **Standard Fine-tuning:** Direct fine-tuning from pre-trained BERT weights for 3 epochs.
- **Unlearning + Fine-tuning:** 3 epochs of training with randomly shuffled labels (maintaining class balance), followed by 3 epochs of standard fine-tuning.

Optimization. Both protocols use AdamW optimizer with learning rate 2×10^{-5} and weight decay 0.01, batch size 32. No learning rate warmup or scheduling is applied. Training uses cross-entropy loss over the 4 classes.

MI Computation. MI is computed 24 times per epoch (approximately every 200 batches) using 5000 training samples. For standard IB, we use the 4-dimensional logit vector \mathcal{T} from the classification head. For GIB, we use the raw 128-dimensional token ID sequences as input features \mathcal{X} (no PCA is applied). MI estimation uses histogram binning with 30 bins.

E.6 ADVERSARIAL ROBUSTNESS

Architecture. 4-layer fully-connected network: $784 \rightarrow 1024 \rightarrow 20 \rightarrow 20 \rightarrow 20 \rightarrow 10$, with *tanh* activations after each hidden layer and softmax output.

Adversarial Training. FGSM attacks are applied to every training example in each batch: $x_{adv} = x + \epsilon \cdot \text{sign}(\nabla_x \mathcal{L}(f(x), y))$ where $\epsilon \in \{0.01, 0.1, 1.0\}$. Perturbed inputs are clipped to $[0,1]$. The training loss is the average of clean and adversarial losses: $\mathcal{L} = (\mathcal{L}_{clean} + \mathcal{L}_{adv})/2$. No validation set or early stopping is used.

Training Details. Networks are trained for 10,000 epochs using Adam optimizer with learning rate 10^{-3} . MI is computed every 250 epochs between inputs and the final 20-dimensional hidden layer activations using histogram binning (30 bins).

F ALTERNATIVE MI ESTIMATION USING LOSS COMPARISON

To validate the robustness of our findings, we repeated our experiments using an alternative MI estimation method based on predictive power (Covert et al., 2020). This method estimates MI by training a model to predict one variable from another and measuring the predictive performance. For discrete targets, we use cross-entropy loss to directly recover the MI in bits. For continuous targets, we use mean squared error (MSE) loss, which provides an approximate MI estimate. While this approach is more computationally intensive than histogram binning, it can potentially capture more complex dependencies.

F.1 ACTIVATION FUNCTION COMPARISON

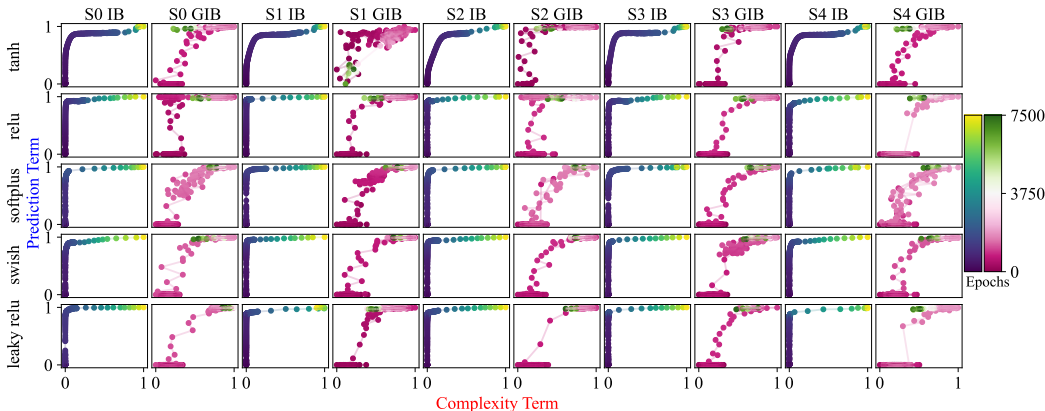


Figure 8: Information plane dynamics across activation functions using loss comparison method MI estimation. Standard IB (blue) and GIB (pink) trajectories for networks trained on synthetic tasks S0-S4. MI computed every 10 epochs for first 2000 epochs, then every 250 epochs.

Figure 8 shows information plane dynamics using loss comparison estimation. While compression phases are less clearly defined than with histogram binning, we observe that only our GIB formulation (pink trajectories) exhibits compression phases across the different activation functions. The standard IB (blue trajectories) shows minimal or no compression, consistent with our main findings. The reduced clarity of phases likely stems from the increased variance inherent in the loss comparison method, which requires training auxiliary models at each measurement point.

F.2 SIMPLE MATHEMATICAL FUNCTIONS

Figure 9 presents results for networks learning arithmetic and polynomial functions. For the addition task, we observe some compression phases in our GIB formulation but not in the standard IB. However, for the remaining functions (multiplication and symmetric polynomials), the information plane trajectories show no clear phase structure for either method. This is likely due to two factors: (1) the use of MSE loss for continuous targets provides only approximate MI estimates, and (2) the reduced sampling frequency (every 10 epochs) may miss rapid transitions. The computational cost of loss comparison necessitated this reduced sampling rate, as each MI estimate requires training an auxiliary model.

F.3 RESNET INFORMATION DYNAMICS

Figure 10 reveals an interesting pattern in ResNet training dynamics. The standard IB (blue trajectories) typically shows a clear fitting phase (upward movement) but often lacks a subsequent compression phase. In contrast, our GIB formulation (pink trajectories) exhibits the opposite behavior: less pronounced fitting phases but more consistent compression. This asymmetry suggests that loss comparison estimation may be more sensitive to the synergistic decomposition in our GIB formulation than to the aggregate information flow measured by standard IB.

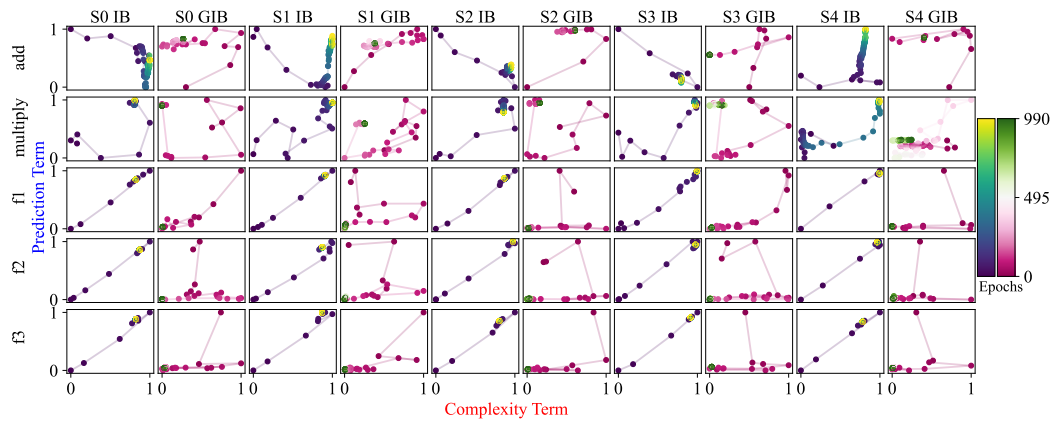


Figure 9: Information plane dynamics for simple mathematical functions using loss comparison MI estimation. Due to computational constraints, MI was computed every 10 epochs rather than continuously.

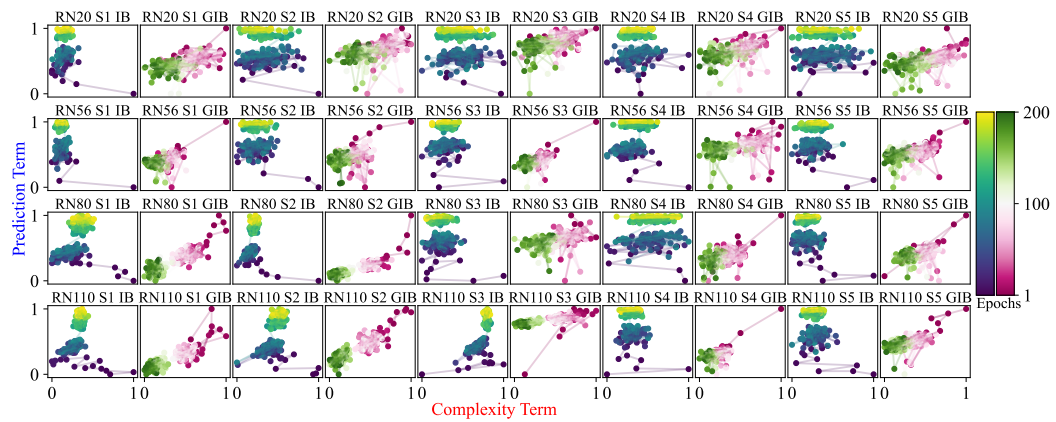


Figure 10: Information plane dynamics for ResNets on CIFAR-10 using loss comparison MI estimation. MI computed at every epoch using the same PCA preprocessing as in main experiments.

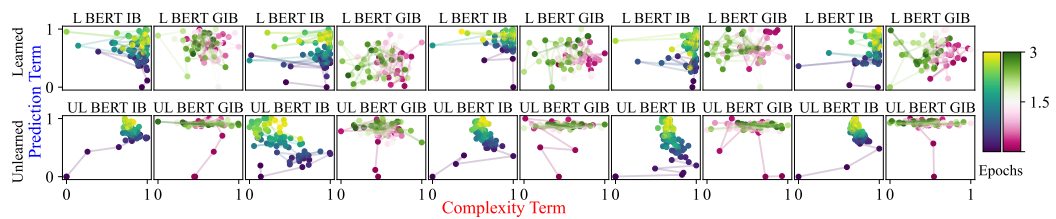


Figure 11: Information plane dynamics for BERT fine-tuning using loss comparison MI estimation. Top row shows standard fine-tuning (Learned), bottom row shows unlearning followed by fine-tuning (Unlearned).

F.4 BERT FINE-TUNING DYNAMICS

Figure 11 examines BERT fine-tuning with loss comparison estimation. Before the unlearning intervention (top row), both IB and GIB trajectories are difficult to interpret, showing erratic patterns without clear phase structure. After unlearning (bottom row), the dynamics become more structured: both methods consistently show fitting phases across all seeds. However, only the GIB formulation exhibits a compression phase, and this is clearly visible only for seed 1. The increased noise in these measurements compared to histogram binning may reflect the challenge of estimating MI in high-dimensional token spaces using loss comparison.

F.5 SUMMARY OF LOSS COMPARISON RESULTS

While loss comparison provides a theoretically principled approach to MI estimation, our results demonstrate several practical limitations. The method produces noisier estimates than histogram binning, particularly for continuous targets and high-dimensional inputs. Despite this increased noise, our GIB formulation was still more likely to exhibit compression phases compared to standard IB, which often showed only fitting phases or no clear dynamics at all. This robustness is particularly notable given the well-documented brittleness of information plane dynamics. As demonstrated by Saxe et al. (2019) and later by Geiger (2022), observing clear compression phases in the standard IB framework depends critically on the choice of activation functions, binning procedures, and even random initialization. The fact that our GIB formulation shows more consistent phase structure across different MI estimation methods may suggest that synergy-based decomposition captures a more fundamental aspect of how neural networks process information during learning.

G COMPUTATIONAL COMPLEXITY

The computational requirements of GIB and IB differ significantly in their scaling behavior. If we define our unit of computation as a single MI estimation, GIB requires $2N + 1$ calculations: more specifically, one for the prediction term $I(\mathcal{X}; Q(Z, Y))$ and $2N$ for the complexity term (computing $I(\mathcal{X}^{-i}; Q(Z, Y))$ and $I(X^i; Q(Z, Y))$ for each feature). Critically, these calculations occur at the input layer where dimensionality is typically highest, for CIFAR-10, this means 3072 features. However, GIB’s computational cost is independent of network depth, since it only considers input-output relationships. In contrast, standard IB requires $2L$ MI calculations for L layers, computing $I(\mathcal{X}; \mathcal{T}_l)$ and $I(\mathcal{T}_l; Y)$ at each layer. While one might compute IB only for the final layer where dynamics are often most pronounced, this prevents the use of the IB as a tool for understanding learning dynamics throughout the network. Additionally, GIB benefits from a key advantage: we can apply PCA to high-dimensional inputs (as we do for CIFAR-10 in Section 5.2) because features at the input layer share a common representation space (Turk & Pentland, 1991). Conversely, combining representations across layers for IB is less conventional.

H EFFECT OF PCA DIMENSIONALITY ON GIB DYNAMICS

Figure 12 demonstrates the impact of PCA dimensionality on observed GIB dynamics. With only 25 principal components, the compression phases are absent; trajectories show limited leftward movement and often remain clustered. However, as we increase to 50 components (shown in main results) and then to 100 components, the compression phases become increasingly apparent. This progression suggests that capturing synergistic information requires sufficient dimensionality to represent the complex feature interactions present in the original input space.

I SUM VERSUS WHOLE SYNERGY FORMULATION

I.1 SUM-VERSUS-WHOLE SYNERGY

In this section, we examine an alternative formulation of synergy based on sum versus whole synergy rather than our feature-wise approach. Due to the increased noise in this estimation method, all MI values are averaged over 50 iterations to obtain stable measurements.

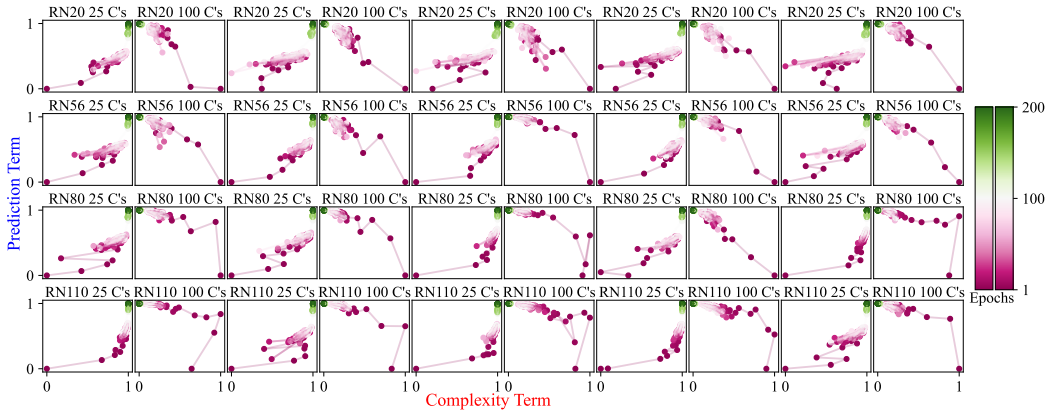


Figure 12: GIB information plane dynamics for ResNets with varying PCA dimensionality. Each subplot shows results for KPCA with 25 (left) versus 100 (right) components (C’s). As dimensionality increases, compression phases become more pronounced.

This alternative definition of GIB is based on the sum-versus-whole formulation of synergy, which compares information available from the complete feature set against the sum of information from individual components (Schneidman et al., 2003). The basic form is $\text{Syn}_{\text{GIB}}(\mathcal{X} \rightarrow Y) = I(\mathcal{X}; Y) - \sum_{i=1}^N (I(X^i; Y))$, which considers only individual features. This captures the intuitive notion of synergy, for example, XOR has zero information from individual inputs but perfect information from their combination, yielding maximal synergy (Bell, 2003). Unlike exponentially complex PID-based measures (Williams & Beer, 2010), this formulation requires only $O(N)$ mutual information calculations, making it computationally feasible for tracking synergistic learning dynamics in high-dimensional neural networks. Combining this with our representation of the PMI-weighted combination of Z and Y and rewriting as a Lagrangian optimization we get the following:

$$\mathcal{L}_{\text{svw}} = \max_{p(Z|X)} \left[\underbrace{I(\mathcal{X}; Q(Z, Y))}_{\text{prediction term}} - \beta^{-1} \underbrace{\sum_{i=1}^N I(X^i; Q(Z, Y))}_{\text{complexity term}} \right] \quad (22)$$

In the following section, we compare the outcomes of tracking this optimization with those obtained from the approach introduced in the main paper.

I.2 ACTIVATION FUNCTION COMPARISON

Figure 13 shows that the alternative synergy formulation (SVW) improves upon standard IB by exhibiting compression phases in several cases where IB fails. However, the compression is less pronounced and less consistent across activation functions compared to our feature-wise GIB. This suggests that while any synergy-based decomposition provides benefits over treating the latent space as a black box, the specific choice of synergy might impact the observability of information dynamics.

I.3 SIMPLE MATHEMATICAL FUNCTIONS

For NNs learning simple mathematical functions (Figure 14), the alternative synergy formulation consistently exhibits compression phases across all tasks. This represents a substantial improvement over standard IB, which shows no compression for these functions.

I.4 RESNET INFORMATION DYNAMICS

Figure 15 shows that the alternative synergy formulation reveals distinct phases in ResNet training.

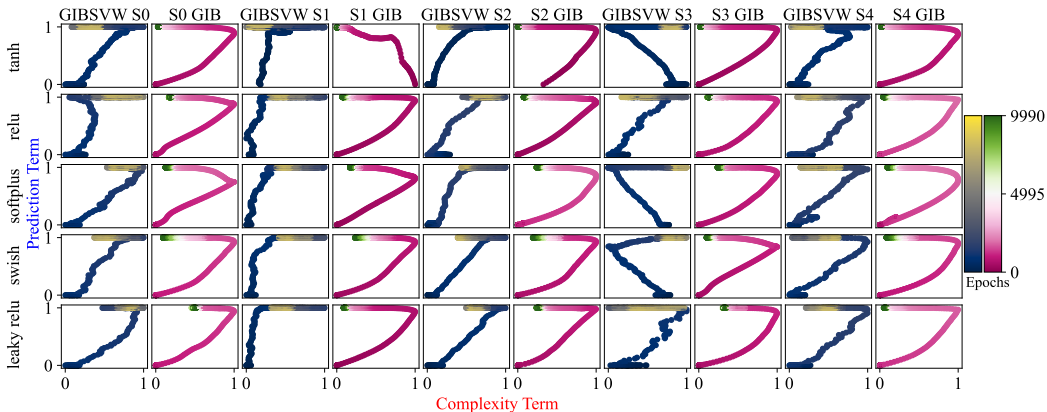


Figure 13: Information plane dynamics comparing the alternative synergy bottleneck (SVW, blue) with our GIB (pink) across multiple activation functions. While SVW shows compression phases more frequently than standard IB, it exhibits less consistent compression than our feature-wise GIB formulation. MI values averaged over 50 iterations.

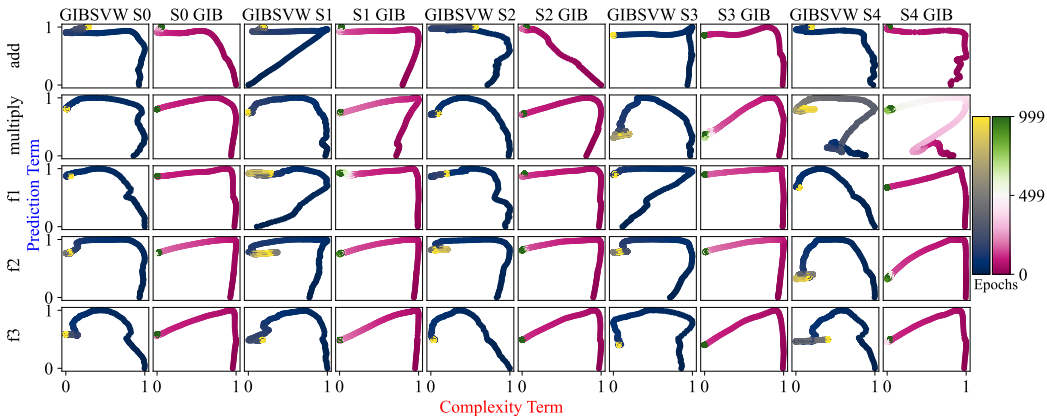


Figure 14: Learning dynamics for simple mathematical functions. The alternative synergy bottleneck (SVW) consistently shows compression phases across all functions, significantly outperforming standard IB.

I.5 BERT FINE-TUNING DYNAMICS

The first notable limitation of the alternative synergy formulation appears in transformer fine-tuning (Figure 16). The SVW method fails to exhibit compression phases for BERT on the AG News classification task, even after our unlearning intervention. In contrast, our GIB formulation clearly reveals compression dynamics. This discrepancy suggests that variance-weighted synergy measures may struggle to capture the high-dimensional, attention-based computations characteristic of transformers.

I.6 SUMMARY

The alternative synergy formulation serves as a useful baseline, showing that synergy-based approaches generally outperform standard IB.

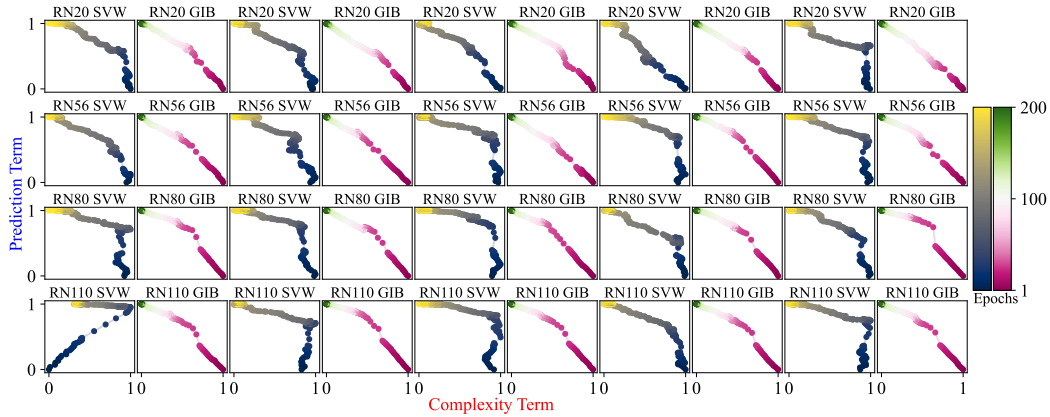


Figure 15: ResNet information dynamics on CIFAR-10. The alternative synergy bottleneck (SVW) shows distinct compression and non-compression phases, providing clearer learning dynamics than standard approaches while exhibiting more variability than our feature-wise GIB.

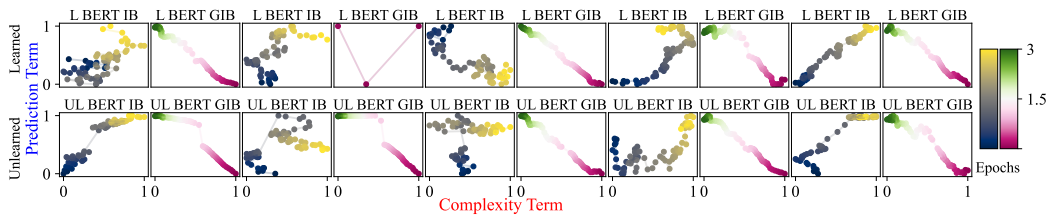


Figure 16: BERT fine-tuning with the alternative synergy bottleneck. Unlike our GIB formulation, SVW fails to show compression phases for both standard fine-tuning and the unlearning protocol, suggesting inherent limitations in capturing synergistic dynamics in transformer architectures.